Fluorinated CYTOP passivation effects on the electrical reliability of multilayer MoS_2 field-effect transistors

2015 Nanotechnology 26 455201

(http://iopscience.iop.org/0957-4484/26/45/455201)

IOP Publishing Nanotechnology
Nanotechnology 26 (2015) 455201 (7pp) doi:10.1088/0957-4484/26/45/455201

Fluorinated CYTOP passivation effects on the electrical reliability of multilayer MoS_2 field-effect transistors

Jeongkyun Roh[1], In-Tak Cho[1], Hyeonwoo Shin[1], Geun Woo Baek[2], Byung Hee Hong[3], Jong-Ho Lee[1], Sung Hun Jin[2] and Changhee Lee[1]

[1] Department of Electrical and Computer Engineering, Inter-University Semiconductor Research Center, Seoul National University, 1 Gwanak-ro, Gwanak-gu, Seoul 151-742, Korea
[2] Department of Electronic Engineering, Incheon National University, Academy-ro, Yeongsu-gu, Incheon 406-772, Korea
[3] Department of Chemistry, Seoul National University, 1 Gwanak-ro, Gwanak-gu, Seoul 151-742, Korea

E-mail: shjin@inu.ac.kr and chlee7@snu.ac.kr

Received 18 June 2015, revised 9 September 2015
Accepted for publication 11 September 2015
Published 16 October 2015

Abstract

We demonstrated highly stable multilayer molybdenum disulfide (MoS_2) field-effect transistors (FETs) with negligible hysteresis gap ($\Delta V_{HYS} \sim 0.15$ V) via a multiple annealing scheme, followed by systematic investigation for long-term air stability with time (~50 days) of MoS_2 FETs with (or without) CYTOP encapsulation. The extracted lifetime of the device with CYTOP passivation in air was dramatically improved from 7 to 377 days, and even for the short-term bias stability, the experimental threshold voltage shift, outstandingly well-matched with the stretched exponential function, indicates that the device without passivation has approximately 25% larger the barrier distribution ($\Delta E_B = k_B T_o$) than that of a device with passivation. This work suggests that CYTOP encapsulation can be an efficient method to isolate external gas (O_2 and H_2O) effects on the electrical performance of FETs, especially with low-dimensional active materials like MoS_2.

Keywords: molybdenum disulfide, CYTOP passivation, field-effect transistors

1. Introduction

Among the various two-dimensional (2D) nanomaterials, transition metal dichalcogenides (TMDCs) have recently received tremendous attention and been actively researched as another opportunity in electronic applications beyond the Si era because of their novel electrical, [1–3] optical, [4] and chemical properties [5, 6]. In particular, their sizable direct (or indirect) bandgap property, unlike graphene, as well as an ultra-thin form of layers for TMDCs are two of the most appealing aspects for applications of next-generation field-effect transistors (FETs), [1, 7, 8] photodetectors, [4, 9] chemical and gas sensors, [5, 10] and nonvolatile memory cells [11, 12]. As a result, many research activities based on TMDCs in this field have been reported up to now.

However, one of the key limitations for TMDC devices, like other types of low-dimensional material, comes from the intrinsic nature of instability associated with easy adsorption of gaseous molecules such as oxygen and moisture due to the large surface areas of low-dimensional materials [13–15]. Even though several studies, adopting plasma-enhanced chemical vapor deposition (PECVD) [14], atomic layer deposition (ALD) [16], and PMMA passivation [17] for the improvement of instability of TMDC devices have been reported, their approaches have several drawbacks, as they require a relatively high temperature process (~350 °C), are not cost-effective, have a non-ideal surface chemistry of passivation layers, and are prone to easy permeation of moisture. Furthermore, using one of the representative hydrophobic polymers, CYTOP passivation has recently been reported to improve the stability of TMDC FETs and optical sensors in diodes [18]. However, their evaluations on electrical characteristics for the effectiveness of CYTOP passivation were very limited, thereby not fully enlightened in the aspects of reliability (or longevity) in air and bias temperature instability when CYTOP passivation was adopted.

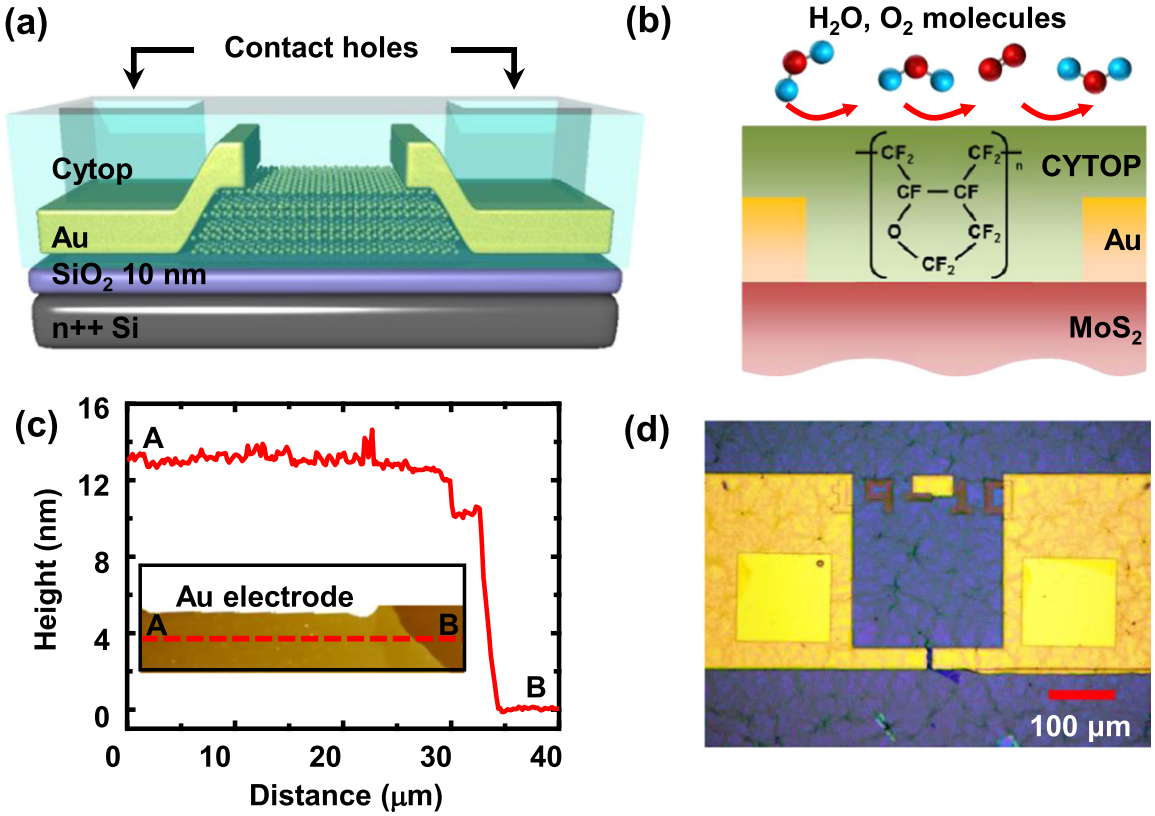

Figure 1. (a) A perspective view of the multilayer MoS_2 FETs with fluorinated polymer CYTOP passivation. (b) Schematic to explain a conceptual model for blocking water and oxygen molecules by CYTOP passivation. (c) AFM profile to show the thickness (∼13 nm) of the multilayer MoS_2 flakes. A and B denote the positions where the MoS_2 channel and gate dielectric (∼SiO_2) are located, respectively. (d) An optical microscope image of the fabricated MoS_2 FETs after contact opening process. The device has physical dimensions of (W/L∼30/10 μm).

In this study, we systemically evaluated the effects of CYTOP passivation for molybdenum disulfide (MoS_2) FETs as one of the representative TMDCs, for two aspects in particular. The first is to isolate the origins of device instability, coming from either internal device issues or external environmental issues; for the validation of this issue, we first implemented highly stable MoS_2 FETs with negligible hysteresis gaps ($\Delta V_{HYS} \sim 0.15$ V), indicating low defect levels were included in the device itself, via multiple annealing schemes and then, the long-term stability of MoS_2 FETs with (or without) passivation in air were evaluated by tracking electrical properties up to 50 days. Furthermore, the bias stability of the MoS_2 FETs with (or without) passivation was directly investigated by analyzing short-term reliability. For the validation of CYTOP passivation effects, their electrical parameters such as electrical field-effect mobility, contact resistance, device life time, the characteristic trapping time, and the energy barrier distribution for the multilayer MoS_2 FETs with (or without) passivation were extracted and compared accordingly.

2. Methods

Figure 1(a) shows a perspective view of the multilayer MoS_2 FETs passivated with CYTOP (CTL-809M, Asahi Glass Co., Ltd) which has been employed as an excellent inhibitor for permeation of moisture (or/and oil) due to a hydrophobic, fluorinated ending group as indicated in figure 1(b) [19–21]. An n-type silicon wafer with heavy phosphorus doping ($\rho \sim 0.005$ ohm cm) was used as a starting substrate, followed by dry oxidation at 950 °C. Multilayers of molybdenum disulfide (MoS_2) were mechanically exfoliated from bulk MoS_2 crystals (SPI Supplies, 429ML-AB) by using poly dimethylsioxane (PDMS) elastomer, subsequently transferred onto Si substrates with 10 nm thick thermal-oxide. For the evaluation of layer thickness of MoS_2, atomic force microscopy (AFM, Park system, XE-100) analysis as shown in figure 1(c) was performed and the typical thickness of multi layers of MoS_2 turned out to be within the range of 13 nm which approximately corresponds to 20 layers. Then, each sample was annealed in a mixed gas (∼Ar/H_2) for one hour at 400 °C for desorption of carbon residues or/and water molecules associated with the exfoliation process. Photolithographic patterning and thermal evaporation of Au (∼50 nm), followed by lift-off in acetone, created source and drain electrodes on multilayer MoS_2 with good Ohmic contact [1, 22]. After forming S/D electrodes, additional annealing, with the same condition as the first annealing, was executed to remove PR residues or/and adsorbed water molecules, typically contaminated during photolithography and the lift-off process. Each sample contains at least more than 10 devices

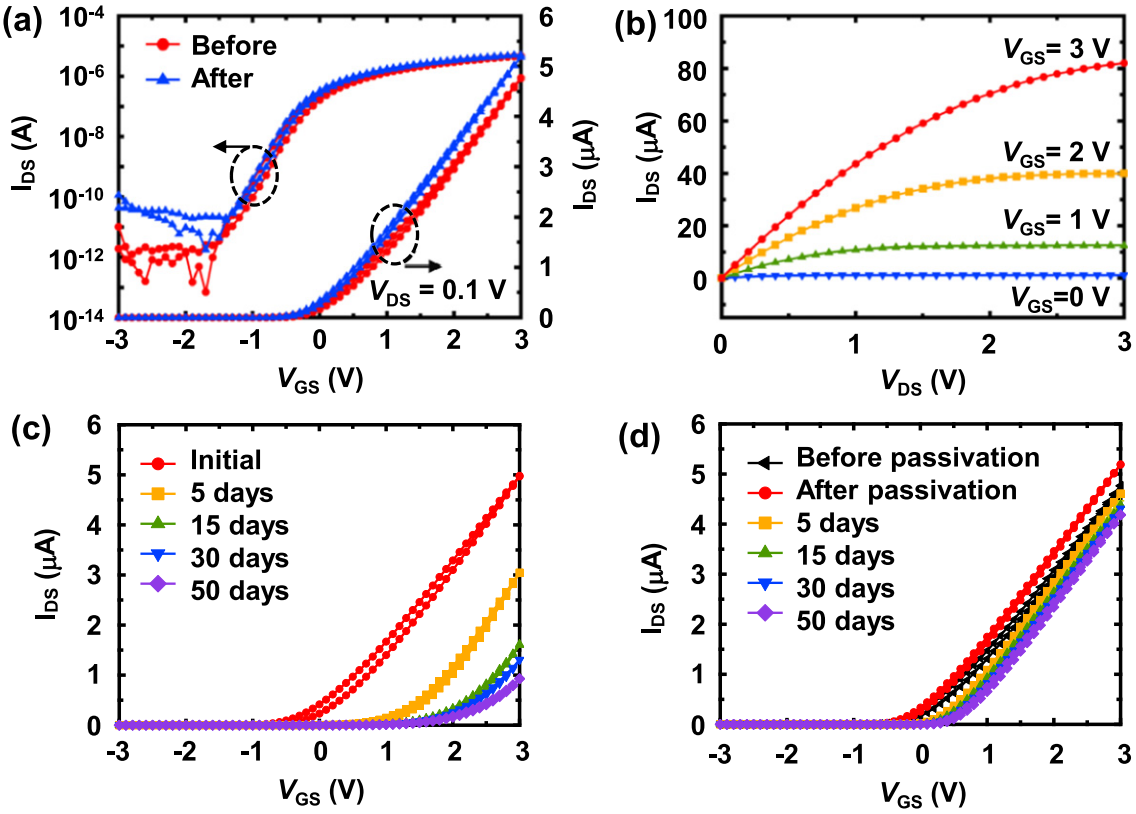

Figure 2. (a) Transfer characteristics of the MoS_2 FETs before and after CYTOP passivation. Circle (●) and triangle (▲) symbols indicate the device before and after CYTOP passivation, respectively. The electrical measurements were performed in a linear regime at $V_{DS} = 0.1$ V. (b) Output characteristic of the MoS_2 FETs with CYTOP passivation. Transfer characteristics of the MoS_2 FETs (c) without and (d) with CYTOP passivation as the time stored in air at room temperature increases. All electrical characteristics were measured in air.

with the same physical dimensions of channel length ($L_{ch} \sim 10\ \mu$m) on the same substrate. The electrical characteristic for each device was measured by using a precision semiconductor parameter analyzer (Agilent, B1500A). The back channel of MoS_2 FETs was passivated by a fluorinated polymer CYTOP ($t_{CYTOP} \sim 400$ nm) with a typical spin coating process, immediately followed by annealing at 100 °C for 1 h in a vacuum oven. Finally, CYTOP film over the source and drain electrodes as shown in figure 1(d) was etched away by using plasma etching as reported elsewhere [23].

3. Results and discussion

Figure 2(a) shows the transfer characteristics of the multilayer MoS_2 FETs with a ratio of width to length ($W/L = 30/10\ \mu$m) before and after CYTOP passivation. The transfer characteristics at a drain-to-source voltage (V_{DS}) of 0.1 V were measured before CYTOP passivation followed by consecutively measured *I–V* properties right after passivation of CYTOP on the same device. As shown in figure 2(a), the multilayer MoS_2 FETs even before passivation show a negligible hysteresis gap ($\Delta V_{HYS} = 0.14$ V), indicating that the optimized annealing process via a multiple annealing scheme leads to the elimination of possible candidates of traps on the surface of the multilayers of MoS_2 associated with absorbates (i.e., moisture or/and carbon residues) [15, 24]. Also, the MoS_2 FETs show good switching properties with a subthreshold slope (*SS*) of 247 mV dec^{-1} and on/off ratio of $\sim 10^7$. Furthermore, there was no noticeable degradation observed in turn-on regime even after passivation, and the extracted field-effect mobility (μ_{eff}) and threshold voltage (V_{TH}) of the multilayer MoS_2 FETs after passivation are 16.8 $cm^2\ V^{-1}\ s^{-1}$ and −0.04 V, which are similar to the values before passivation, respectively. Each field-effect mobility (μ_{eff}) before and after passivation in the linear regime was extracted at a maximum point of transconductance ($g_{m_max} \sim 1.75\ \mu$S) according to $\mu_{eff} = g_m L \times (WC_{ox}V_{DS})^{-1}$, where C_{ox} and g_m are the gate insulator capacitance per unit area and the transconductance, respectively. However, in the off-current regime, a slightly increased off-current right after CYTOP passivation was observed and then relieved back to the initial off-current level (∼a few pA) one day later, which is speculated to come from temporal charge generation and relaxation effects in the CYTOP layer, [18, 19] typically observed after encapsulation of the fluorinated polymers [25, 26]. Figure 2(b) shows output characteristics of the MoS_2 FET after passivation. The device showed typical n-type modulation properties as gate-to-source voltage (V_{GS}) increased from 0 V to 3 V and a good saturation behavior was observed in an operation regime of saturation, indicating the device itself after passivation retained its virgin characteristics before passivation.

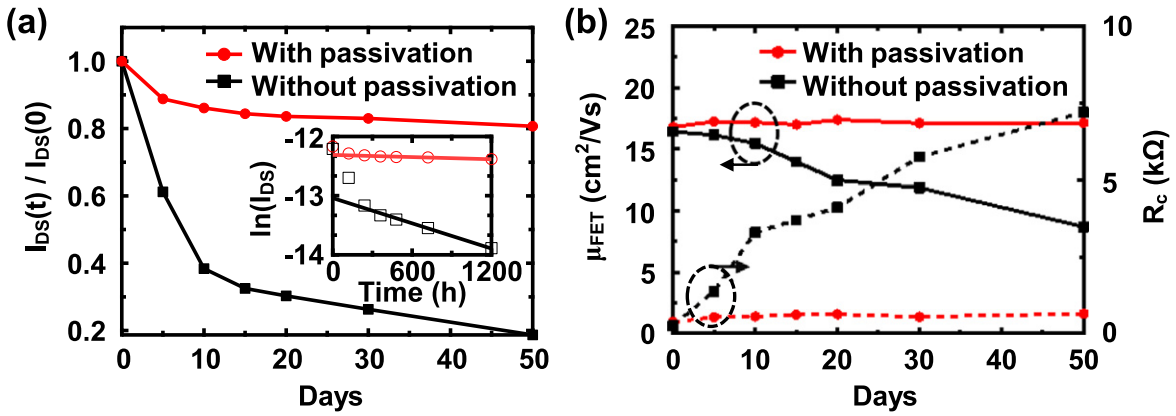

Figure 3. (a) Normalized drain-to-source current (I_{DS}) behavior with time for the MoS_2 FETs with (or without) CYTOP passivation. Each value (I_{DS}) was extracted with time at a bias condition (i.e., $V_{GS} = 3$ V, $V_{DS} = 0.1$ V). I_{DS} (0) indicates the initial current level ($t = 0$ s). The inset denotes the semi-logarithmic plots for log (I_{DS}) versus time and each solid line in the inset corresponds to its extrapolated line. The time constant for the device with (or without) passivation is $\gamma_{w/} = 6.1 \times 10^{-5}$ s (or $\gamma_{w/o} = 4 \times 10^{-3}$ s), respectively. (b) Electrical evolution of field-effect mobility (μ_{eff}) and contact resistance (R_c) for MoS_2 FETs with (● solid circle) and without (■ solid square) CYTOP passivation with time stored in air. Lines and dash lines indicate μ_{eff} and R_c, respectively.

For the evaluation of CYTOP passivation effects on longevity (or long-term stability) of the MoS_2 FETs, the multilayer MoS_2 FETs were fabricated and selected as having similar both its flake thickness (∼13 nm) and electrical characteristics (∼16 cm^2 V^{-1} s^{-1}, on/off ratio > 10^6) initially, followed by CYTOP passivation. The MoS_2 FETs with (or without) passivation were stored in ambient air. The electrical characteristics for each device were measured with time up to 50 days in air. Figures 2(c) and (d) show that the transfer characteristics for the representative MoS_2 FETs without and with passivation with time, respectively. Overall, the devices without passivation show huge degradation in on-current and large threshold voltage shift toward positive direction, whereas the passivated MoS_2 FETs showed slight current reduction, but the sub-threshold slope (*SS*) with time was mostly consistent within the error range of experimental measurement. In addition, the same trend for the passivation effects on the MoS_2 FETs were consistently observed for all other devices (∼ at least more than 5 devices) on the same sample.

For a more quantitative analysis for both of the devices in degradation, normalized current level with time was depicted in figure 3(a) and their current degradation behavior in the inset of figure 3(a) was also replotted in a semi-logarithmic scale, indicating exponential decay of drain current with time [27] so that it can be analytically expressed as $I_{DS}(t) = I_{DO} \exp(-\gamma t)$, where I_{DO} is the initial on-current in air with (or without) passivation and γ is the slope obtained from the plot of log(I_{DS}) versus time as shown in the inset of figure 3(a). The extracted values of γ for both of the devices are 6.1×10^{-5} (with passivation) and 4.0×10^{-3} (without passivation). The lifetimes, extracted as the time when the on-current has deteriorated to half of the initial current for both of the devices, are 377 days (with passivation) and 7 days (without passivation), respectively. In addition, for the analysis of CYTOP passivation effects on electrical performance of the MoS_2 FETs, field-effect mobility (μ_{eff}) and contact resistance (R_c) with time were extracted and compared for both of the devices stored in air. For the estimation of the electrical contact properties, contact resistance (R_c) was extracted by using the Y-function method reported elsewhere [28–30]. Figure 3(b) shows that field-effect mobility (μ_{eff}) and contact resistance (R_c) for the MoS_2 FETs with passivation remains consistently within the experimental error range (∼4%) with time in air. On the other hand, as the exposure time in air increases, the MoS_2 FETs without passivation shows noticeable degradation of field-effect mobility (μ_{eff}) from 16.2 cm^2 V^{-1} s^{-1} to 8.7 cm^2 V^{-1} s^{-1} and a significant increase of contact resistance (R_c) from 0.26 kΩ to 7.3 kΩ. The noticeable decrease of field-effect mobility (μ_{eff}) with time is mainly attributed to the chemisorption of oxygen or/and water molecules on the back channel of MoS_2, which could act as local Coulomb scatters for the accumulated charge (i.e., electron) centroid nearly located in the front channel. In addition, the increase of contact resistance (R_c) with time is speculated to come from the increase of Schottky barrier (∼ϕ_{SB}) between MoS_2 and Au associated with the increase of effective work function (∼ϕ_m) of Au which is near S/D contact regions due to chemisorption of oxygen [31] on the surface of contact regions of MoS_2 (∼ϕ_s). Therefore, the dramatic reduction of lifetime for the MoS_2 FETs without passivation is mainly ascribed to both the noticeable deterioration of field-effect mobility (μ_{eff}) and the significant increase of contact resistance (R_c) associated with chemisorption (or/and penetration) of oxygen or/and water molecules, predominantly on the back surface of MoS_2. The analyses on field-effect mobility (μ_{eff}) and contact resistance (R_c) extracted from figure 3 suggest that the CYTOP passivation for MoS_2 FETs can be an efficient method to prevent oxygen or/and water molecules from penetrating into channel areas of MoS_2 FETs, which leads to reliable operation in air.

The effect of CYTOP passivation on bias stability in air can be a key aspects to investigate for the evaluation of reliability of MoS_2 FETs. For the investigation of bias stress effects, MoS_2 FETs were implemented and their electrical properties showed field-effect mobility ($\mu_{eff} \sim 22$ cm^2 V^{-1} s^{-1}), threshold

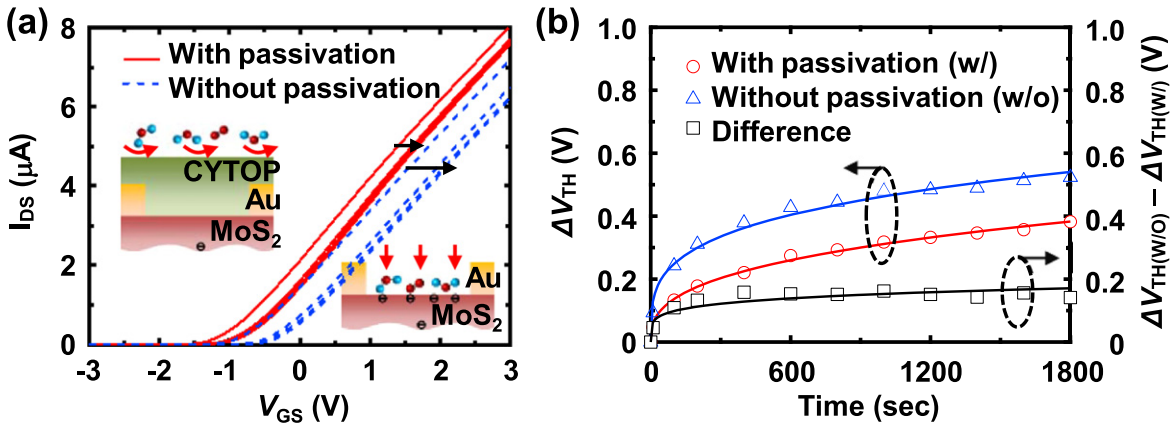

Figure 4. (a) Transfer characteristics of the MoS_2 FETs with (or without) CYTOP passivation with stress time. Electrical bias of $V_{GS} = 3$ V, $V_{DS} = 0$ V was applied to the device for 1800 s at the substrate temperature of $T_{sub} = 60$ °C. The schematics in the inset indicate conceptual models to explain gas adsorption for the device with (or without) CYTOP encapsulation. (b) Electrical evolution of threshold voltage shift of the MoS_2 FETs with (or without) CYTOP passivation with stress time. ΔV_{TH}(w/) and ΔV_{TH}(w/o) correspond to the threshold voltage shift for the device with (○; open circle) and without (△; open triangle) CYTOP encapsulation, respectively.

voltage ($V_{TH} \sim -0.58$ V), and high on/off ratio ($\sim 10^7$), respectively. To examine the effects of bias stress, we applied a gate-to-source voltage (V_{GS}) of +3 V to the MoS_2 FETs with (or without) passivation while holding drain-to-source voltage (V_{DS}) at 0 V, as shown in figure 4(a). During the bias temperature stress, the substrate temperature and effective stress time were fixed as 60 °C and 1800 s, respectively. To avoid device variation effects on reliability characteristics of MoS_2 FETs, the bias stress was first applied to the MoS_2 FETs without passivation, and then all the electrical characteristics were analyzed, followed by baking at 150 °C for 30 min in a glove box to promote the recovery of electrical characteristics to the virgin state. After confirmation of the recovery of electrical characteristics for the MoS_2 FETs, subsequent CYTOP passivation was performed, and then the same stress conditions were applied to the same device with passivation. Figure 4(a) indicates the evolution of transfer characteristics for each MoS_2 FET with (or without) passivation. The behaviors of threshold voltage shifts (ΔV_{TH}) are noticeably different; the threshold voltage shift (ΔV_{TH} (w/) (or ΔV_{TH} (w/o))) for the MoS_2 FETs with (or without) passivation after bias stress test is 0.38 V (or 0.52 V), respectively. To gain some insight, we analyzed the behaviors of threshold voltages depending on stress time for the MoS_2 FETs with (or without) passivation as shown in figure 4(b). Typically, the bias stress-induced threshold voltage shift (ΔV_{TH}) can be described by a stretched exponential time (t)-dependent formula applicable to thin film transistors based on a wide variety of disordered [32–35] or/and organic crystalline systems; [36]

$$\left|\Delta V_{TH}(t)\right| = \left|V_{GS} - V_{TH}(0)\right| \times \left[1 - \exp\left\{-(t/\tau)^{\beta}\right\}\right] \quad (1)$$

where $\tau = \tau_o \exp(E_\tau / k_B T)$ represents the characteristic trapping time of carriers in which τ_o is a thermal prefactor, E_τ the average effective barrier for emission, T substrate temperature, and β is a dispersion parameter. V_{GS} and $V_{TH}(0)$ are the applied gate bias stress and initial threshold voltage, respectively. The value of the dispersion parameter (β) is related to the distribution of the activation energy for charge trapping ($\Delta E_B = k_B T/\beta$) where k_B is the Boltzmann constant. Typically, the energy structure of each trap site can be described by E_τ (i.e., the mean barrier height) and the barrier distribution ($\Delta E_B = k_B T_o$) [37]. Even though the validity of this model (i.e., equation (1)) to the system of MoS_2 FETs is not yet clear, and needs to be studied separately later, the electrical fittings for the experimental threshold voltage shifts are outstandingly well-fitted, as assessed by its coefficient of determination [38] ($R^2 \sim 0.994$ for with and 0.976 for without passivation, respectively) and the extracted values of the barrier distribution for the MoS_2 FETs with (or without) passivation correspond to 7.76×10^{-2} eV (or 1.02×10^{-1} eV). The data suggest that the barrier distribution for the device without passivation is about 25% that of device with passivation. This difference is, at least partly, a consequence of chemisorption of oxygen and water molecules on the back channel of the MoS_2 FETs which results in the increase of the chance for trapping of electrons in the back channel. In addition, the graph (square symbols) in figure 4(b), representing the difference of a threshold voltage shift (ΔV_{TH}) for each device with (or without) passivation, shows a reasonably good fit with equation (1); the extracted values of threshold voltage shift (ΔV_{TH}), characteristic trapping time (τ) and dispersion parameter (β) are 0.14 V, 2.2×10^9 s and 0.2, respectively. Moreover, the barrier distribution ($\Delta E_B = k_B T_o$) for the curve (square symbols) was extracted as 1.43×10^{-1} eV which is about 40% larger than that of the device without passivation. This suggests that the increased barrier distribution ($\Delta E_B = k_B T_o$) is probably associated with the net effects of back channel regions where the events of trapping might occur via trap sites with wide barrier distribution due to external gases (i.e., O_2 and H_2O). Notice that subtraction of the values which are extracted for each device with (or without) passivation conceptually reflects the pure portion of back channel region in terms of trapping events, on the assumption that CYTOP passivation

perfectly prevents external gases (i.e., O_2 and H_2O) from permeation into the back channel. For thin film transistors, the gate bias instability is typically a result of charge trapping in a gate insulator, at the interface between insulator and semiconductor, and in a semiconductor itself. In the case of the MoS_2 FETs, among the several aforementioned attributes of origins for device instability, the back channel portion can be much more pronounced due to charge trapping on the back channel region of the MoS_2 FETs, ascribed by easy adsorbed water or/and oxygen molecules. This is attributed to the nature of a high surface-to-volume ratio of the 2D structure and hydrophilicity of the MoS_2 surface [13, 14].

4. Conclusion

In summary, we implemented multilayer MoS_2 FETs with a negligible hysteresis gap via multiple annealing schemes, and the device instability issues associated with internal (i.e., gate dielectric, interface of semiconductor and dielectrics, and contact properties) and external (i.e., gas ambient effects) attributes were systematically analyzed by investigating lifetimes in air and short-term bias instabilities for the devices with (or without) passivation of CYTOP. For the quantitative analyses on device degradation in air, field-effect mobility (μ_{eff}) and contact resistance (R_c) with time were extracted, and the results indicate that the noticeable degradation of field-effect mobility (μ_{eff}) and increase of contact resistance (R_c) for the device without passivation in air could be one of main causes of current degradation. Furthermore, the short-term reliability for the devices with (or without) passivation were analytically evaluated by using both stretched exponential decay formula and experimental threshold voltage shift (ΔV_{TH}), and their characteristics trapping time (τ), dispersion parameter (β), and energy barrier distribution ($\Delta E_B = k_B T_o$) indicate that external effects, associated with O_2 and H_2O, possibly increase the energy distribution of energy barrier, which results in fast decay in the early stage of current–voltage behaviors. In addition, CYTOP passivation could be a good candidate for achieving long-term and short-term reliability of MoS_2 FETs based on a cost-effective, low-temperature process scheme, enlightening the feasibility of usage of different types of 2D materials including graphene and other TMDC materials for the envisioned applications.

Acknowledgments

This work was supported by the Human Resources Development Program of the Korea Institute of Energy Technology Evaluation and Planning (KETEP) grant funded by the Korea government Ministry of Trade, Industry and Energy (No. 20124010203170) and Basic Science Research Program through the National Research Foundation of Korea (NRF) funded by the Ministry of Science, ICT & Future Planning (NRF-2014R1A1A1038274).

References

[1] Radisavljevic B, Radenovic A, Brivio J, Giacometti V and Kis A 2011 Single-layer MoS_2 transistors *Nat. Nanotechnology* **6** 147–50
[2] Radisavljevic B and Kis A 2013 Mobility engineering and a metal–insulator transition in monolayer MoS_2 *Nat. Mater.* **12** 815–20
[3] Yoon Y, Ganapathi K and Salahuddin S 2011 How good can monolayer MoS_2 transistors be? *Nano Lett.* **11** 3768–73
[4] Lopez-Sanchez O, Lembke D, Kayci M, Radenovic A and Kis A 2013 Ultrasensitive photodetectors based on monolayer MoS_2 *Nat. Nanotechnology* **8** 497–501
[5] Perkins F K, Friedman A L, Cobas E, Campbell P M, Jernigan G G and Jonker B T 2013 Chemical vapor sensing with monolayer MoS_2 *Nano Lett.* **13** 668–73
[6] Late D J *et al* 2013 Sensing behavior of atomically thin-layered MoS_2 transistors *ACS Nano* **7** 4879–91
[7] Kim S *et al* 2012 High-mobility and low-power thin-film transistors based on multilayer MoS_2 crystals *Nat. Commun.* **3** 1011
[8] Cheng R, Jiang S, Chen Y, Liu Y, Weiss N, Cheng H-C, Wu H, Huang Y and Duan X 2014 Few-layer molybdenum disulfide transistors and circuits for high-speed flexible electronics *Nat. Commun.* **5** 5143
[9] Yin Z, Li H, Li H, Jiang L, Shi Y, Sun Y, Lu G, Zhang Q, Chen X and Zhang H 2012 Single-Layer MoS_2 Phototransistors *ACS Nano* **6** 74–80
[10] Li H, Yin Z, He Q, Li H, Huang X, Lu G, Fam D W H, Tok A I Y, Zhang Q and Zhang H 2012 Fabrication of single- and multilayer MoS_2 film-based field-effect transistors for sensing NO at room temperature *Small* **8** 63–7
[11] Bertolazzi S, Krasnozhon D and Kis A 2013 Nonvolatile memory cells based on MoS_2/graphene heterostructures *ACS Nano* **7** 3246–52
[12] Wang J, Zou X, Xiao X, Xu L, Wang C, Jiang C, Ho J C, Wang T, Li J and Liao L 2015 Floating gate memory-based monolayer MoS_2 transistor with metal nanocrystals embedded in the gate dielectrics *Small* **11** 208–13
[13] Qiu H, Pan L, Yao Z, Li J, Shi Y and Wang X 2012 Electrical characterization of back-gated bi-layer MoS_2 field-effect transistors and the effect of ambient on their performances *Appl. Phys. Lett.* **100** 123104
[14] Late D J, Liu B, Matte H S S R, Dravid V P and Rao C N R 2012 Hysteresis in single-layer MoS_2 field effect transistors *ACS Nano* **6** 5635–41
[15] Cho K, Park W, Park J, Jeong H, Jang J, Kim T-Y, Hong W-K, Hong S and Lee T 2013 Electric stress-induced threshold voltage instability of multilayer MoS_2 field effect transistors *ACS Nano* **7** 7751–8
[16] Na J *et al* 2014 Low-frequency noise in multilayer MoS_2 field-effect transistors: the effect of high-k passivation *Nanoscale* **6** 433–41
[17] Park W, Park J, Jang J, Lee H, Jeong H, Cho K, Hong S and Lee T 2013 Oxygen environmental and passivation effects on molybdenum disulfide field effect transistors *Nanotechnology* **24** 095202
[18] Jeon P J, Min S-W, Kim J S, Raza S R A, Choi K, Lee H S, Lee Y T, Hwang D K, Choi H J and Im S 2015 Enhanced device performances of WSe_2-MoS_2 van der Waals junction p-n diode by fluoropolymer encapsulation *J. Mater. Chem. C* **3** 2751–8
[19] Choi S-H, Jang J-H, Kim J-J and Han M-K 2012 Low-temperature organic (CYTOP) passivation for improvement of electric characteristics and reliability in IGZO TFTs *IEEE Electron Device Lett.* **33** 381–3
[20] Chung D S, Lee J-S, Huang J, Nag A, Ithurria S and Talapin D V 2012 Low voltage, hysteresis free, and high

mobility transistors from all-inorganic colloidal nanocrystals *Nano Lett.* **12** 1813–20

[21] Granstrom J, Swensen J S, Moon J S, Rowell G, Yuen J and Heeger A J 2008 Encapsulation of organic light-emitting devices using a perfluorinated polymer *Appl. Phys. Lett.* **93** 193304

[22] Kaushik N, Nipane A, Basheer F, Dubey S, Grover S, Deshmukh M M and Lodha S 2014 Schottky barrier heights for Au and Pd contacts to MoS_2 *Appl. Phys. Lett.* **105** 113505

[23] Cho I-T, Kim J I, Hong Y, Roh J, Shin H, Baek G W, Lee C, Hong B H, Jin S H and Lee J-H 2015 Low frequency noise characteristics in multilayer WSe_2 field effect transistor *Appl. Phys. Lett.* **106** 023504

[24] Li T, Du G, Zhang B and Zeng Z 2014 Scaling behavior of hysteresis in multilayer MoS_2 field effect transistors *Appl. Phys. Lett.* **105** 093107

[25] Seo S-m Jang C-H and Park J-H 2008 Influence of passivation with non-charged fluorinated ethylene propylene on the properties of pentacene organic thin film transistor *Org. Electron.* **9** 899–902

[26] Park S, Nam S, Kim L, Park M, Kim J, An T K, Yun W M, Jang J, Hwang J and Park C E 2012 Synthesis and characterization of a fluorinated oligosiloxane-containing encapsulation material for organic field-effect transistors, prepared via a non-hydrolytic sol–gel process *Org. Electron.* **13** 2786–92

[27] Han S H, Kim J H, Jang J, Cho S M, Oh M H, Lee S H and Choo D J 2006 Lifetime of organic thin-film transistors with organic passivation layers *Appl. Phys. Lett.* **88** 073519

[28] Ghibaudo G 1988 New method for the extraction of MOSFET parameters *Electron. Lett.* **24** 543–5

[29] Kwon H-J, Kim S, Jang J and Grigoropoulos C P 2015 Evaluation of pulsed laser annealing for flexible multilayer MoS_2 transistors *Appl. Phys. Lett.* **106** 113111

[30] Kwon H-J, Jang J, Kim S, Subramanian V and Grigoropoulos C P 2014 Electrical characteristics of multilayer MoS_2 transistors at real operating temperatures with different ambient conditions *Appl. Phys. Lett.* **105** 152105

[31] Derycke V, Martel R, Appenzeller J and Avouris P 2002 Controlling doping and carrier injection in carbon nanotube transistors *Appl. Phys. Lett.* **80** 2773–5

[32] Mathijssen S G J, Cölle M, Gomes H, Smits E C P, de Boer B, McCulloch I, Bobbert P A and de Leeuw D M 2007 Dynamics of threshold voltage shifts in organic and amorphous silicon field-effect transistors *Adv. Mater.* **19** 2785–9

[33] Lee W H, Choi H H, Kim D H and Cho K 2014 25th anniversary article: microstructure dependent bias stability of organic transistors *Adv. Mater.* **26** 1660–80

[34] Banger K K, Yamashita Y, Mori K, Peterson R L, Leedham T, Rickard J and Sirringhaus H 2011 Low-temperature, high-performance solution-processed metal oxide thin-film transistors formed by a 'sol–gel on chip' process *Nat. Mater.* **10** 45–50

[35] Osedach T P, Zhao N, Andrew T L, Brown P R, Wanger D D, Strasfeld D B, Chang L-Y, Bawendi M G and Bulović V 2012 Bias-stress effect in 1,2-Ethanedithiol-treated PbS quantum dot field-effect transistors *ACS Nano* **6** 3121–7

[36] Barra M, Di Girolamo F V, Minder N A, Gutiérrez Lezama I, Chen Z, Facchetti A, Morpurgo A F and Cassinese A 2012 Very low bias stress in n-type organic single-crystal transistors *Appl. Phys. Lett.* **100** 133301

[37] Choi H H, Lee W H and Cho K 2012 Bias-stress-induced charge trapping at polymer chain ends of polymer gate-dielectrics in organic transistors *Adv. Funct. Mater.* **22** 4833–9

[38] Colléaux F, Ball J M, Wöbkenberg P H, Hotchkiss P J, Marder S R and Anthopoulos T D 2011 Bias-stress effects in organic field-effect transistors based on self-assembled monolayer nanodielectrics *Phys. Chem. Chem. Phys.* **13** 14387–93